第 16 卷 第 2 期 高 压 物 理 学 报 Vol. 16, No. 2
2002 年 6 月 CHINESE JOURNAL OF HIGH PRESSURE PHYSICS June, 2002

Article ID: 1000-5773(2002)02-0094-11

PENETRATION AND PERFORATION OF THICK METALLIC TARGETS UNDER IMPACT BY MISSILES*

H. M. Wen

(*Laboratory for Mechanical Behaviour and Design of Materials, University of Science and Technology of China, Hefei* 230027, *China*)

Abstract: Simple analytical equations are given in this paper to predict the penetration and perforation of thick metallic targets under normal impact by missiles with different nose shapes over a wide range of impact velocities. In the formulation, it is assumed that the deformations are localized and that the impact energy is dissipated only by penetration. It is further assumed that the mean pressure offered by the target materials to resist the missiles consists of two parts. The first is a cohesive quasi-static resistive pressure due to the elastic-plastic deformation of the target materials based upon a cavity expansion formula. The second is a dynamic resistive pressure defined as a velocity-dependent enhancement factor applied to the quasi-static resistance. Equations are derived for predicting the D. O. P. (Depth of Penetration) in the targets and the ballistic limits in the case of perforation. It transpires that the model predictions are in good agreement with experimental data for a wide range of metallic targets struck transversely by missiles with different nose shapes over a wide range of impact velocities.

Key words: impact; penetration; perforation; metallic targets; missiles; ballistic limit

CLC number: O385 **Document code**: A

1 Introduction

The penetration and perforation of targets by missiles involve highly complex processes, which have been investigated experimentally for more than two centuries and analytically during the last few decades. Accounts of this work can be found in the reviews by Backman and Goldsmith[1], Zukas[2], Anderson and Bodner[3] and Corbett, Reid and Johnson[4]. Depending on impact velocity, the material and geometric properties of both the projectile and the target, several theoretical models (Analytical and Numerical) have been proposed over the years to predict the level of the penetration in thick targets or the impact conditions for the perforation of plates as can be seen from these reviews. However, many of the analytical models are single-mechanism models which have so far enjoyed limited applications. Numerical simulations have been successful in predicting the response of targets to projectile impact but, unfortunately, considerable resources in terms of computing time (CPU) are still required. On the other hand, from the engineering point of view there is considerable interest in the development of empirical or semi-empirical laws for the penetration and perforation of plates as noted in References[1,4,5].

* **Received date**: 2001-12-24; **Revised date**: 2002-02-05

Biography: H. M. Wen(1965—), man, professor.

In this paper, simple semi-empirical equations are derived for the penetration and perforation of thick metallic targets by rigid missiles with conical, ogival and spherical noses as well as eroding long rod penetrators. Theformulation is based upon the assumption that the deformations are localized and the impact energies are dissipated only by penetration. It is further assumed that the average pressure provided by the target materials to resist the projectiles can be divided into two parts. One part is the cohesive static resistive pressure applied normally to the projectile surface due to the elastic-plastic deformations of the target material associated with cavity expansion. The other is the dynamic resistive pressure arising from velocity effects. The latter is simply expressed as a velocity-dependent enhancement factor applied to the static pressure term. Correlations between the equations and experimental data are presented and discussed. The basic approach is a pragmatic one which seems to have broad applications. The model can be used to predict the penetration and perforation of targets struck transversely by rigid projectiles with different nose shapes as well as eroding long rod penetrators over a wide range of impact velocities. It transpires that the model predictions are in good agreement with experimental data.

2 Formulation of the Problem

2.1 Assumption about the Resistive Pressure

It is assumed that the mean pressure (σ) applied normally to the surface of the missile by a metallic target to resist penetration and perforation by a missile can be decomposed into two parts, one part is the cohesive static resistive pressure (σ_s) due to the elastic-plastic deformations of the target material and the other is the dynamic resistive pressure (σ_d) arising from velocity effects. Thus[6]

$$\sigma = \sigma_s + \sigma_d \tag{1}$$

Ifit is further assumed that $\sigma_s = \alpha\sigma_t$, σ_d is a function of the parameter $(\rho_t/\sigma_t)^{1/2} v_i$, $\sigma_d = \beta(\rho_t/\sigma_t)^{1/2} v_i \sigma_t$, then Equation (1) can be rewritten as

$$\sigma = \left(\alpha + \beta\sqrt{\rho_t/\sigma_t}\ v_i\right)\sigma_t \tag{2}$$

where σ_t is a measure of the quasi-static target material strength. ρ_t and v_i are the density of the target material and the initial impact velocity of the missile respectively. α, β are constants which are determined either theoretically or experimentally.

The resistive pressure is generally expected to be a function (usually a polynomial function) of the penetration velocity, as noted in References[1,7]. In Equation (2), the mean pressure provided by the target material to resist the missile is simply taken as a linear function of the initial impact velocity. α in Equation (2) represents the constraining effect of the material surrounding the missile, which inhibits the flow of the target material as it is displaced by the missile during penetration. It may be determined theoretically by the spherical or cylindrical cavity expansion analysis[8] for elastic-plastic materials such as metals.

2.2 Penetration of Semi-infinite Metal Targets

Fig. 1 shows the geometries of rigid missiles with conical or ogival noses. The missile is assumed to have density ρ_p and mass m with diameter d (or radius a). l and l_n are the lengths of the shank and nose for conical and ogival projectiles respectively, as shown in Figs. 1(b) and 1(a). If a rigid projectile has a complex configuration (for example, it is hollow or has a sabot system) then the projectile still can be described as one of those depicted in Fig. 1 but with an effective density (ρ_p^e). ρ_p^e is taken to

be the ratio of the projectile mass to the volume of the basic configuration as shown in Fig. 1. Fig. 1 (a) shows the ogive profile as the arc of a circle that is tangent to the projectile shank. It is also common to define the ogive in terms of calibre-radius-head, viz.

$$\mathrm{CRH}=S/(2a)=\Psi \tag{3}$$

where S and a are defined in Fig. 1(a).

Fig. 2 shows the impact of a rigid projectile with a conical nose on a metal target at normal incidence with an initial impact velocity v_i. Two situations may arise, as shown in Fig. 2. One is that the final depth of penetration has not reached the shoulder of the projectile and the other is that the final depth of penetration is larger than the nose length. Similar situations may occur for rigid projectiles with spherical or ogival noses impacting a metallic target. Equations are derived in the following sections for the depth of penetration into targets by rigid missiles with different nose shapes.

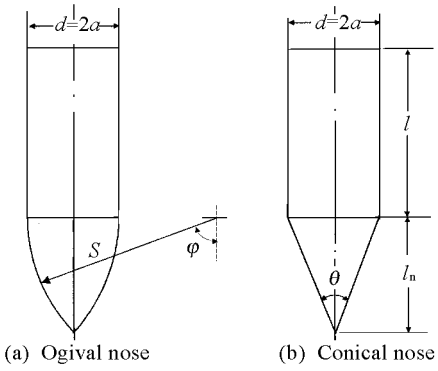

Fig. 1 Projectile geometries

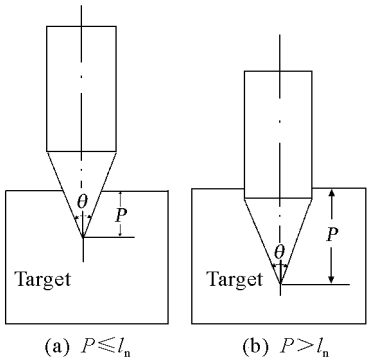

Fig. 2 Schematic diagrams of a conical-nosed projectile impacting on semi-infinite targets

2.2.1 Conical-nosed Missiles

2.2.1.1 Case I: $P\leqslant l_n$

For a rigid conical-nosed projectile, the motion and the final depth of penetration can be calculated if the resistive forces are known. The resistive force of a conical-nosed projectile penetrating a metal target at normal incidence as shown in Fig. 2(a) can be written as

$$f=\sigma A \tag{4}$$

where f is the resistive force and σ is the mean resistive pressure provided by the target material and is defined by Equation (2). A is the instant cross-sectional area and can be determined from the geometrical configuration depicted in Fig. 2(a), i. e.,

$$A=\pi P^2\tan^2(\theta/2) \tag{5}$$

in which θ and P are the cone angle and the depth of penetration respectively. Substituting Equations (2) and (5) into Equation (4) gives

$$f=\pi P^2\tan^2(\theta/2)\sigma_t\left(\alpha+\beta\sqrt{\rho_t/\sigma_t}\ v_i\right) \tag{6}$$

From energy conservation, one obtains

$$E_k=\int_0^P f\mathrm{d}P \tag{7}$$

where E_k is the initial kinetic energy of the projectile. Substituting Equation (6) into the above equation yields

$$E_k=\left[P^3A_0\sigma_t/(3l_n^2)\right]\left(\alpha+\beta\sqrt{\rho_t/\sigma_t}\ v_i\right) \tag{8}$$

after using $\tan(\theta/2) = a/l_n$. Here $A_0 = \pi a^2$ (a is the missile radius) is the cross-sectional area of the projectile shank. Substituting $E_k = (1/2)mv_i^2$ (m is the missile mass) into Equation (8) and rearranging gives

$$P/(l + l_n/3) = (\rho_p/\rho_t)(\rho_t v_i^2/\sigma_t)\left[(2/3)\left(\alpha + \beta\sqrt{\rho_t/\sigma_t}\ v_i\right)(P/l_n)^2\right]^{-1} \tag{9}$$

after using $m = A_0(l + l_n/3)\rho_p$.

2.2.1.2 Case II: $P > l_n$

As shown in Fig. 2(b), the penetration process can be divided into two stages. The first stage when $P \leqslant l_n$ has been described in the previous section. For the second stage when $P > l_n$, the resistive force (f) can be written as

$$f = A_0\sigma = A_0\sigma_t\left(\alpha + \beta\sqrt{\rho_t/\sigma_t}\ v_i\right) \tag{10}$$

after using Equation (2). From energy consideration, one obtains

$$E_k = \int_0^{l_n} f\,dP + \int_{l_n}^{P} f\,dP \tag{11a}$$

Substituting Equations (6) and (10) into Equation (11a) and rearranging yields

$$E_k = \left[P - (2/3)l_n\right]A_0\sigma_t\left(\alpha + \beta\sqrt{\rho_t/\sigma_t}\ v_i\right) \tag{11b}$$

Substituting $E_k = (1/2)mv_i^2$ into the above equation and using $m = A_0(l + l_n/3)\rho_p$ gives the final depth of the penetration

$$P/\left(l + l_n/3\right) = (\rho_p/\rho_t)(\rho_t v_i^2/\sigma_t)\left[2\left(\alpha + \beta\sqrt{\rho_t/\sigma_t}\ v_i\right)\right]^{-1} + 2\left(3l/l_n + 1\right)^{-1} \tag{12}$$

2.2.2 Ogival-nosed Missiles

Similarly, Equations (13) and (14) can be obtained for the final depth of penetration into a metal target by a rigid projectile with ogival nose.

2.2.2.1 Case Ⅰ: $P \leqslant l_n$

$$\rho_p(l + 8\psi^3\eta\mu)v_i^2 = 16\psi^3 a\sigma\Big\{-\cos\varphi + (1/3)\cos^3\varphi - \left[\varphi - (1/2)\sin 2\varphi\right]\sin\varphi_0 - \sin^2\varphi_0\cos\varphi_0 + (\pi/2)\sin\varphi_0 + \eta\Big\} \tag{13a}$$

$$P = \left(\sqrt{4\psi - 1} - 2\psi\cos\varphi\right)a \tag{13b}$$

in which φ is defined in Fig. 1(a) and the mean resistive pressure σ is determined by Equation (2). φ_0 and η are evaluated by the following equations

$$\varphi_0 = \sin^{-1}\left[(2\psi - 1)/(2\psi)\right] \tag{13c}$$

$$\eta = -(\pi/2)\sin\varphi_0 + \cos\varphi_0 - (1/3)\cos^3\varphi_0 + \left[\varphi_0 - (1/2)\sin 2\varphi_0\right]\sin\varphi_0 + \sin^2\varphi_0\cos\varphi_0 \tag{13d}$$

2.2.2.2 Case Ⅱ: $P > l_n$

$$P/(l + 8\psi^3\eta\mu) = (\rho_p/\rho_t)(\rho_t v_i^2/\sigma_t)\left[2\left(\alpha + \beta\sqrt{\rho_t/\sigma_t}\ v_i\right)\right]^{-1} + \left(\sqrt{4\psi - 1} - 8\psi^3\eta\right)a/\left(l + 8\psi^3\eta\mu\right) \tag{14}$$

2.3 Perforation of Finite Plates

The ballistic limit condition for a metal plate with finite thickness struck transversely by a rigid missile with conical, flat, ogival or hemispherical noses can be estimated by the energy balance method. Generally speaking, a fraction of the plate material on the distal side will be ejected due to the surface effects such as spalling or adiabatic shear plugging, depending on the plate material and the test conditions. In other words, the effective thickness (H_e) of the plate will be smaller than the original plate thickness (H), i.e.,

$$H_e = H - \zeta d \tag{15}$$

where $\zeta \geqslant 0$, which is to be determined empirically. There are three phases of penetration for a rigid missile with conical nose impacting on a finite plate. First, the nose enters the plate, second, the nose is fully embedded and finally, the nose exits the plate. The same arguments can also apply to the rigid projectiles with spherical or ogival noses. Following the energy balance method and the procedure outlined in Ref. [6], it shows that

$$E_k = \pi a^2 (H - \zeta d)\sigma_t \left(\alpha + \beta\sqrt{\rho_t/\sigma_t}\ v_c\right) \tag{16a}$$

Substituting $E_k = (1/2)mv_c^2$ into the above equation and rearranging yields

$$v_c = \left[\pi\beta\sqrt{\rho_t\sigma_t}\, d^2 (H - \zeta d)/(4m)\right]\left\{1 + \sqrt{1 + 8\alpha m/\left[\pi\beta^2\rho_t d^2 (H - \zeta d)\right]}\right\} \tag{16b}$$

where v_c is the critical impact velocity or ballistic limit.

3 Correlation with Test Data and Discussion

The equations derived in Section 2 can be compared with experimental data for the penetration and perforation of metal targets by missiles with different nose shapes. The values of the various parameters in the equations have been obtained either theoretically (for example using the cavity expansion analysis[7]) or empirically, which are given in Table 1. σ_y is static yield stress. It is interesting to note that the values of β for metal plates are the same as those for FRP laminates[8].

Table 1 Parameters for metallic targets

Nose shapes	α	β	σ_t	ζ
Conical-nose	$\frac{1}{2}\left[1+\ln\frac{2E}{(5-4v)\sigma_y}\right]$	$2\sin\frac{\theta}{2}$	σ_y	0
Ogival-nose	$\frac{2}{3}\left[1+\ln\frac{E}{3(1-v)\sigma_y}\right]$	$\frac{3}{4\Psi}$	σ_y	0
Hemispherical-nose	$\frac{2}{3}\left[1+\ln\frac{E}{3(1-v)\sigma_y}\right]$	$\frac{3}{2}$	σ_y	0
Eroding penetrators	$\frac{2}{3}\left[1+\ln\frac{E}{3(1-v)\sigma_y}\right]$	$\frac{3}{2}$	σ_y	1

3.1 Conical-nosed Missiles

Fig. 3 shows comparison of the theoretical predictions with the experimental data for 6061-T651 aluminium alloy targets ($\sigma_y = 380$MPa) struck transversely by a 7.1mm diameter conical-nosed projec-

tile with a mass of 23.5g and $\theta = 38.75°$ reported in Reference[9]. The solid and broken lines in the figure are the theoretical predictions by Equations (12) and (9), respectively. Fig. 3 shows that the model predictions (Equations (9) and (12)) are in good agreement with the experimental data in terms of the final depth of penetration.

Fig. 4 shows comparison between the theoretically predicted ballistic limits and the experimental

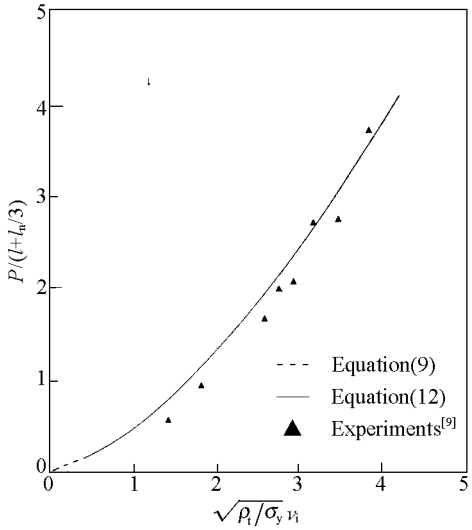

Fig. 3　Comparison of the theoretical predictions with the experimental data for the penetration of 6061-T651 aluminium alloy targets struck by a 7.1 mm conical-nosed projectile with a mass of 23.5g and $\theta = 38.75°$

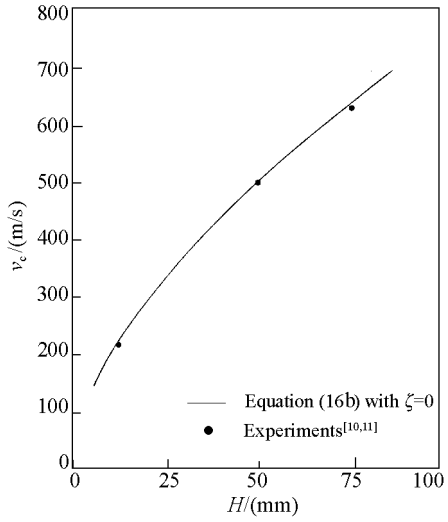

Fig. 4　Comparison of the theoretical predictions with the experimental data for the perforation of 5083-H131 aluminium alloy plates struck by a 8.31mm diameter conical-nosed projectile with a mass of 26g and $\theta = 32.54°$

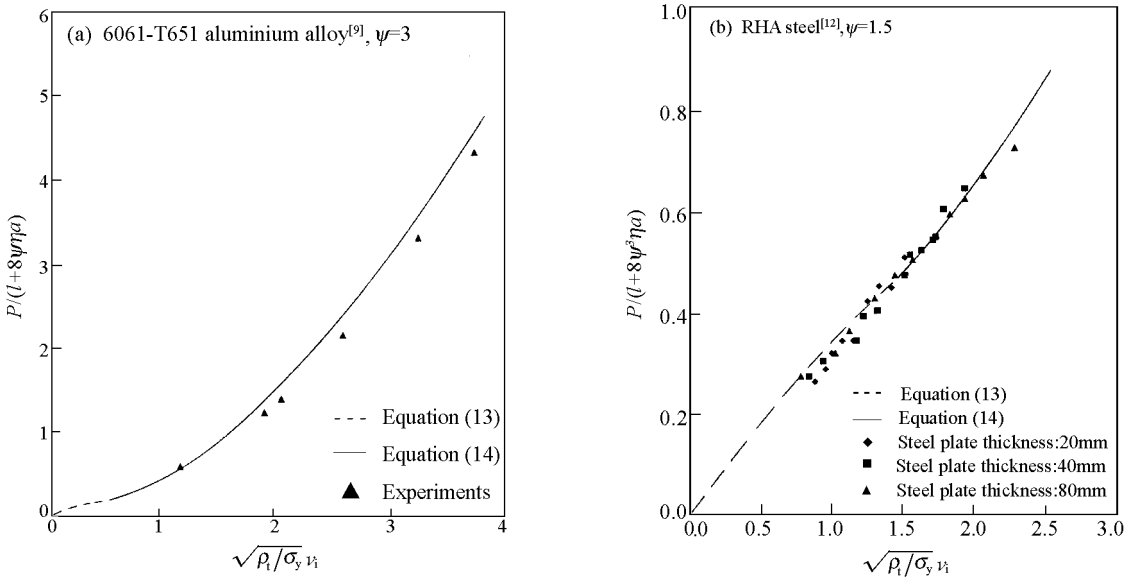

Fig. 5　Comparison of the theoretical predictions with the experimental data for the penetration of targets struck by ogival-nosed missiles

observations for 5083-H131 aluminium armour (σ_y =276MPa) struck normally by a 8.31mm diameter conical-nosed projectile with a mass of 26g and θ= 32.54°[10,11]. Fig. 4 shows evidently that Equation (19b) with ζ= 0 is in good agreement with the experimental data in terms of the ballistic limit.

3.2 Ogival-nosed Missiles

Good agreement is also obtained between the theoretical predictions and the experimental data in Figs. 5(a) and 5(b) for the final depth of penetration of 6061-T651 aluminium alloy targets (σ_y = 380MPa)[9] and high strength steel plates (σ_y = 950MPa)[12] struck by ogival-nosed projectiles with ψ=3 and ψ=1.5 respectively. The solid and broken lines in Figs. 5(a) and 5(b) are those predicted by Equations (14) and (13) respectively.

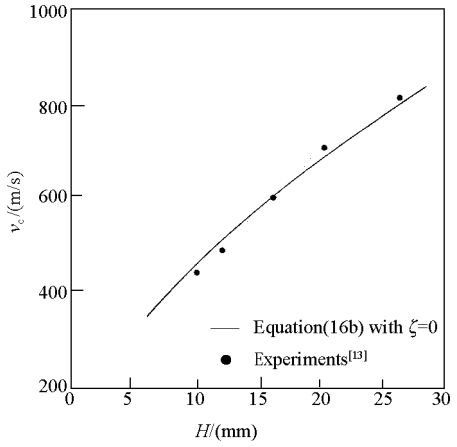

Fig. 6 Comparison of the theoretical predictions with the experimental results for the perforation of mild steel plates struck by an AP projectile

Fig. 6 shows comparison of Equation (16b) with the test results for the perforation of mild steel plates impacted normally by an ogival-nosed AP projectile with ψ=1.5. Equation (16b) with ζ= 0 is in good agreement with the experimental data which were reported in Reference[13].

3.3 Hemispherical-ended Missiles

A hemishperical-ended projectile can be seen as the special case of an ogival-nosed projectile with ψ= 0.5. Hence, the corresponding equations can be recast into the following:

Case Ⅰ: $P \leqslant a$

$$P/(l+2a/3)=(\rho_p/\rho_t)(\rho_t v_i^2/\sigma_t)\left\{2\left(\alpha+\beta\sqrt{\rho_t/\sigma_t}\ v_i\right)\left[P/a-(1/3)(P/a)^2\right]\right\}^{-1} \tag{17}$$

Case Ⅱ: $P > a$

$$P/(l+2a/3)=(\rho_p/\rho_t)(\rho_t v_i^2/\sigma_t)\left[2\left(\alpha+\beta\sqrt{\rho_t/\sigma_t}\ v_i\right)\right]^{-1}+\left(3l/a+2\right)^{-1} \tag{18}$$

Comparisons are made in Figs. 7 and 8 between the theoretical predictions and the experimental data for metal targets struck by rigid projectiles with a spherical nose. The solid and dashed lines in Fig. 7 are the theoretical predictions by Equations (18) and (17) respectively. The solid line in Fig. 8 is predicted by Equation (16b) with ζ=0. Equation (18) is in good agreement with the experimental results for the final depth of penetration of 6061-T651 aluminium alloy targets (σ_y=380MPa) struck by rigid hemispherical-ended projectiles, which were reported in References [9,14] as shown in Fig. 7. Furthermore, Equation(16b) is seen to correlate well with the experimental observations for the perforation of mild steel plates (σ_y= 327MPa)[15] as shown in Fig. 8.

4 Eroding Penetrators

The procedure described in Sections 2 and 3 may also be adapted to predict the penetration and perforation of armour (such as RHA) plates struck by high speed (eroding) long rod KE penetrators. It has been observed experimentally[16,17] that the nose of a projectile mushrooms upon penetrating into a target and that the mushroom head maintains its diameter and is of nearly hemispherical shape

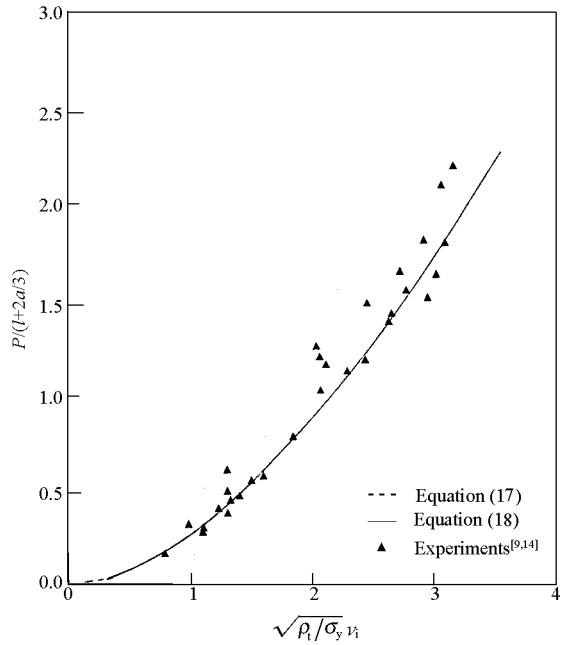

Fig. 7　Comparison of the theoretical predictions with the experimental results for the penetration of 6061-T651 aluminium alloy targets struck by hemispherical-ended projectiles

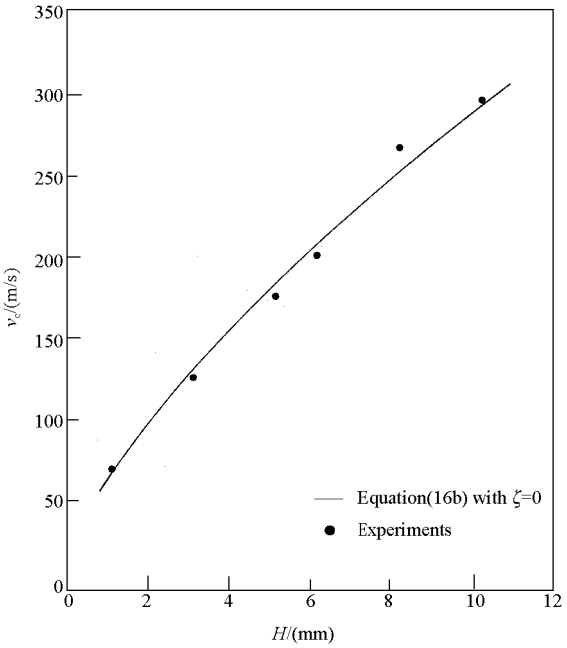

Fig. 8　Comparison of the theoretical predictions with the experimental data for the perforation of mild steel plates struck by hemispherical-ended projectiles

throughout the primary quasi-steady penetration stage. Therefore, the equations derived for the penetration and perforation of targets impacted by a rigid projectile with a spherical nose may be applicable to the problem of RHA plates struck by eroding long rod penetrators by replacing the projectile diameter (or radius) with an effective penetration diameter (or radius), i. e.,

$$P/(l+2a/3)=(\rho_p/\rho_t)(\rho_t v_i^2/\sigma_t)(a/a_e)^2[2(\alpha+\beta\sqrt{\rho_t/\sigma_t}\ v_i)]^{-1}+(a/a_e)/(3l/a+2) \quad (19)$$

and

$$v_c=[\pi\beta\sqrt{\rho_t\sigma_t}\,d_e^2(H-\zeta d)/(4m)]\cdot\{1+\sqrt{1+8\alpha m/[\pi\beta^2\rho_t d_e^2(H-\zeta d)]}\} \quad (20)$$

where d_e (or a_e) is the effective penetration diameter (or radius) and empirically taken to be $1.6d$ for steel armour as compared to a value of $1.55d$ used in Reference[18].

Fig. 9 shows comparison between Equation (19) and the experimental data obtained for the penetration of RHA armour struck by high speed eroding long rod penetrators. ◆, ■ and ▲ repre-

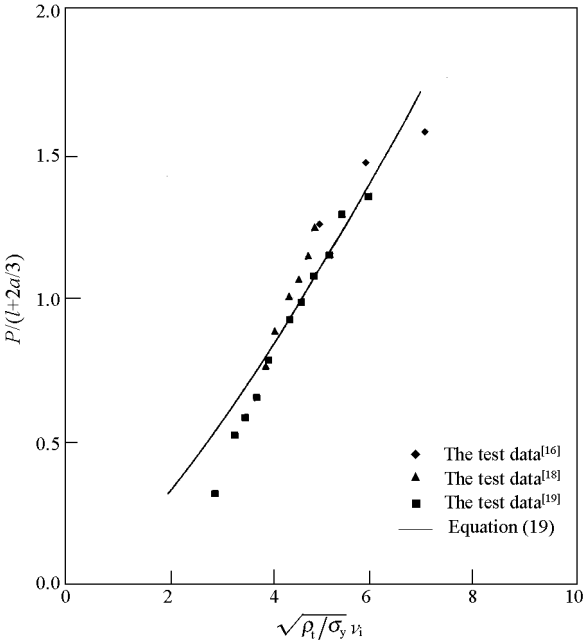

Fig. 9　Comparison of the theoretical predictions with the experimental data for the penetration of RHA steel targets struck by high speed (eroding) long rod penetrators

sent the experiments reported in References [16] (σ_y=1207MPa), [19] (σ_y=1000 MPa) and [18] (σ_y=780 MPa), respectively. Fig. 9 shows that Equation(19) with $d_e=1.6d$ is in good agreement with the experimental results for the non-dimensional parameter $(\rho/\sigma_y)^{1/2}v_i$ ranging from 3 to 7, which corresponds to initial impact velocities ranging from 1km/s to 2.5km/s, approximately. For the non-dimensional parameter less than 3 or greater than 7, Equation(19) predicts not very well as can be seen in Fig. 9. However, it should be expected that the accuracy of the theory(Equation(19)) will be improved if the actual penetration diameter is used in the calculation especially for higher velocity impact.

Comparisons are made in Fig. 10(a) between the theoretical predictions (Equation(20)) and the experimentally obtained ballistic limits for RHA armour plates (σ_y=1200MPa) struck by an eroding long rod penetrator which were examined in Reference[20], while Fig. 10(b) shows comparison of the model predictions with the test data obtained for HHA armour plates (σ_y=1400 MPa) impacted by a high speed long rod penetrator which were investigated in Reference[17]. It is demonstrated in Figs. 10(a) and 10(b) that Equation (20) with $d_e=1.6d$ and $\zeta=1$ is in good agreement with the experimental observations reasonably.

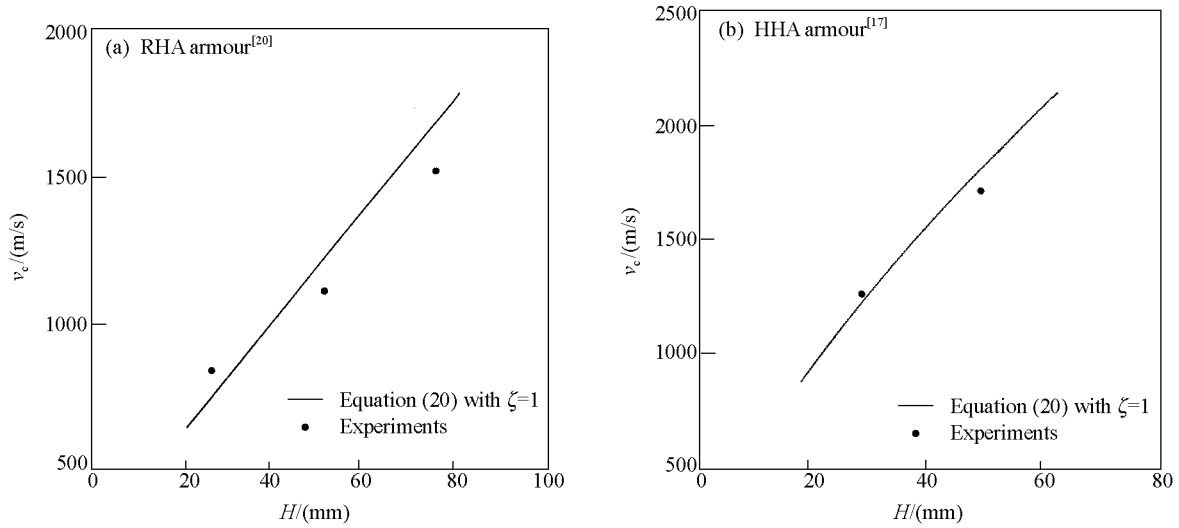

Fig. 10 Comparison of the theoretical predictions with the experimental data for the perforation of steel plates struck by high speed (eroding) long rod penetrators

5 Conclusions

Simple analytical equations have been obtained for the penetration and perforation of thick metallic targets struck transversely by missiles with different nose shapes. The formulation is based on the assumption that the deformations are localized and the impact energies are dissipated only by penetration. It is further assumed that the mean pressure provided by the target materials to resist the projectiles can be decomposed into two parts. One part is the cohesive static resistive pressure due to the elastic-plastic deformations of the target materials, the other is the dynamic resistive pressure arising from the velocity effects.

The theoretical predictions are in good agreement with experimental observations for the final

depth of penetration as well as the ballistic limits for target plates made of a wide range of different metallic materials struck by rigid missiles with conical, ogival or hemispherical noses. By introducing an effective penetration diameter the equations derived for a rigid hemispherical-ended projectile can be used to predict the penetration and perforation of steel armour plates struck by high speed long rod KE penetrators reasonably.

References:

[1] Backman M E,Goldsmith W. The Mechanics of Penetration of Projectile into Targets [J]. Int J Eng Sci,1978,16:1-99.

[2] Zukas J A. Penetration and Perforation of Solids [A]. Zukas J A. Impact Dynamics [C]. New York:John Wiley, 1982. 155-214.

[3] Anderson C E Jr, Bodner S R. Ballistic Impact: The Status of Analytical and Numerical Modelling [J]. Int J Impact Eng,1988,7:9-35.

[4] Corbett G G, Reid S R,Johnson W. Impact Loading of Plates and Shells by Free-Flying Projectiles: A Review [J]. Int J Impact Eng,1996,18(2):141-230.

[5] Wen H M,Jones N. Semi-Empirical Equations for the Perforation of Plates Struck by a Mass [A]. Bulson P S. Structures under Shock and Impact II [C]. Southampton and Boston and Thomas Telford, London:Computational Mechanics Publications,1992. 369-380.

[6] Wen H M. Predicting the Penetration and Perforation of FRP Laminates Struck Normally by Projectiles with Different Nose Shapes [J]. Composite Structures,2000,49:321-329.

[7] Johnson W. Impact Strength of Materials [M]. London:Edward Arnold,1972.

[8] Hill R. The Mathematical Theory of Plasticity [M]. Oxford:Oxford University Press,1950.

[9] Forrestal M J,Okajima K, Luk V K. Penetration of 6061-T651 Aluminium Targets with Rigid Long Rods [J]. ASME J Appl Mech,1988,55:755-760.

[10] Forrestal M J, Rosenberg Z, Luk V K,et al. Perforation of Aluminium Plates with Conical-Nosed Rods [J]. J Appl Mech,1987,54:230-232.

[11] Luk V K, Amos D E. Dynamic Cylindrical Cavity Expansion of Compressible Strain-Hardening Materials [J]. ASME J Appl Mech,1991,58:334-340.

[12] Dikshit S N,Sundararajan G. The Penetration of Thick Steel Plates by Ogive Shaped Projectiles-Experiment and Analysis [J]. Int J Impact Eng,1992,12(3):373- 408.

[13] Gupta N K,Madhu V. Normal and Oblique Impact of a Kinetic Energy Projectile on Mild Steel Plates [J]. Int J Impact Eng,1992,12(3):333-343.

[14] Forrestal M J, Brar N S,Luk V K. Penetration of Strain-Hardening Targets with Rigid Spherical-Nose Rods [A]. Schwer L E. Computational Techniques for Contact, Impact, Penetration and Perforation of Solids [C]. ASME, 1989,AMD-103:215-222.

[15] Corbett G G,Reid S R. Quasi-Static and Dynamic Local Loading of Monolithic Simply-Supported Steel Plates [J]. Int J Impact Eng,1993,13(3):423- 441.

[16] Luk V K,Piekutowski A J. An Analytical Model on Penetration of Erosive Long Rods into Metallic Targets [J]. Int J Impact Eng,1991,11(3):323-340.

[17] Anderson C E Jr, Hohler V,Walker J D,et al. Time-Resolved Penetration of Long Rods into Steel Targets [J]. Int J Impact Eng,1995,16(1):1-18.

[18] Ravid M,Bodner S R,Holcman I. A Two-Dimensional Analysis of Penetration by an Eroding Projectile [J]. Int J

Impact Eng,1994,15(5):587- 603.

[19] Cullis I G,Lynch N J. Performance of Model Scale Long Rod Projectiles against Complex Targets over the Velocity Range 1700～2200 m/s [J]. Int J Impact Eng,1995,17:263-274.

[20] Grace F I. Long-Rod Penetration into Targets of Finite Thickness at Normal Impact [J]. Int J Impact Eng,1995,16(3):419- 433.

厚金属靶在弹丸打击下的侵彻与穿透

文鹤鸣

(中国科学技术大学材料力学行为和设计重点实验室,安徽合肥 230027)

摘要:给出了预测厚金属靶在不同形状弹头弹丸大速度范围内打击下侵彻与穿透的简单分析方程。在方程的建立过程中,假定变形是局部化的、冲击能量仅由侵彻过程吸收,并进一步假定靶材料对弹丸的平均阻(压)力由两部分组成:一部分基于空穴膨胀理论由于靶材料弹-塑性变形所产生的准静态凝聚阻力;另一部分是考虑了速度效应后的动压力。推导出了预测靶侵彻深度和弹道极限的方程表达式,并与金属靶在不同形状弹头弹丸大速度范围内打击下侵彻与穿透的实验进行了比较。理论预测与实验结果吻合得很好。

关键词:冲击;侵彻;穿透;金属靶;弹丸;弹道极限

中图分类号:O385 **文献标识码**:A